

Properties of Galaxies in Cosmic Filaments around the Virgo Cluster

YOUNGDAE LEE,¹ SUK KIM,¹ SOO-CHANG REY,¹ AND JIWON CHUNG²

¹*Department of Astronomy and Space Science, Chungnam National University, Daejeon 34134, Republic of Korea*

²*Korea Astronomy and Space Science Institute 776, Daedeokdae-ro, Yuseong-gu, Daejeon 34055, Republic of Korea*

ABSTRACT

We present the properties of galaxies in filaments around the Virgo cluster with respect to their vertical distance from the filament spine using the NASA-Sloan Atlas catalog. The filaments are mainly composed of low-mass, blue dwarf galaxies. We observe that the $g - r$ color of galaxies becomes blue and stellar mass decreases with increasing vertical filament distance. The galaxies were divided into higher-mass ($\log h^2 M_*/M_\odot > 8$) and lower-mass ($\log h^2 M_*/M_\odot \leq 8$) subsamples. We also examine the $g - r$ color, stellar mass, H α equivalent width (EW(H α)), near-ultraviolet (NUV)– r color, and HI fraction distributions of the two subsamples against the vertical distance. The lower-mass galaxies exhibit a negative $g - r$ color gradient, whereas higher-mass galaxies have a flat $g - r$ color distribution. We observe a negative EW(H α) gradient for higher-mass galaxies, whereas lower-mass galaxies show no distinct EW(H α) variation. In contrast, the $NUV - r$ color distribution of higher-mass galaxies shows no strong trend, whereas the lower-mass galaxies show a negative $NUV - r$ color gradient. We do not witness clear gradients of HI fraction in either the higher- or lower-mass subsamples. We propose that the negative color and stellar mass gradients of galaxies can be explained by mass assembly from past galaxy mergers at different vertical filament distances. In addition, galaxy interactions might be responsible for the contrasting features of EW(H α) and $NUV - r$ color distributions between the higher- and lower-mass subsamples. The HI fraction distributions of the two subsamples suggest that ram-pressure stripping and gas accretion could be ignorable processes in the Virgo filaments.

Keywords: galaxies: dwarf — galaxies: evolution — galaxies: interactions — cosmology: large-scale structure of universe

1. INTRODUCTION

In the frame of the hierarchical structure formation in the standard cold dark matter universe, the build-up of galaxy clusters is characterized by the accretion of galaxies into higher-density cluster environments through filamentary structures (Bond et al. 1996; Springel et al. 2005). It has been proposed that the filament environment around galaxy clusters is closely linked to galaxy evolution in terms of the subject of “pre-processing” (Fujita 2004), where properties of galaxies may already have been altered before they enter galaxy clusters (Zabludoff et al. 1996; De Lucia et al. 2012; Mahajan 2013; Cybulski et al. 2014). Therefore, filaments are ideal places for the investigation of the physical pro-

cesses that control the transitioning of galaxies in less-dense environments to cluster galaxies.

Recently, the specific role of pre-processing in filaments has been extensively explored in different surveys. In particular, there is a growing body of observational evidence indicating that the properties of galaxies (e.g., color, mass, red galaxy fraction, and star-formation rate) change as a function of their distance from the filament spine (e.g., Martínez et al. 2016; Alpaslan et al. 2016; Chen et al. 2017; Kuutma et al. 2017; Malavasi et al. 2017; Mahajan et al. 2018; Kraljic et al. 2018; Bonjean et al. 2019; Luber et al. 2019; Sarron et al. 2019). Galaxies close to filaments show a tendency to have redder colors, lower H α emission-line equivalent width (EW(H α)), and higher early- to late-type galaxy fraction, indicating that the efficiency of star-formation quenching varies with distance from filaments. Furthermore, higher-mass galaxies are preferentially located closer to filaments. These observational results support

Corresponding author: Youngdae Lee; Soo-Chang Rey
 hippo206@gmail.com; screy@cnu.ac.kr

the idea that galaxies could be effectively pre-processed in a moderately dense filament environment.

Several environmental effects are proposed as possible physical mechanisms that could be responsible for the galaxy pre-processing in filaments. Merger and tidal interaction between galaxies are expected to be a prevailing process in the filament environment (Darvish et al. 2015; Malavasi et al. 2017; Kraljic et al. 2018; Mahajan et al. 2018). In addition, stripping of gas within galaxies in filaments can take place by warm-hot intergalactic medium (WHIM; $10^5 \text{ K} < T < 10^7 \text{ K}$, e.g., Benítez-Llambay et al. 2013; see also Tonnesen et al. 2007 for ram-pressure stripping in the cluster periphery) within filaments. As another process, galaxies moving along the filaments can accrete cold gas from intrafilament medium (Kereš et al. 2005; Sancisi et al. 2008; Darvish et al. 2015; Kleiner et al. 2017).

Up to date, most observational studies of filaments have concentrated on massive galaxies with $>10^{10} M_\odot$ mainly due to that filaments are only defined at intermediate and high redshifts. On the other hand, since low-mass ($<10^9 M_\odot$) dwarf galaxies, with low binding energies, are more susceptible to even weak perturbations than massive galaxies, they are a better tool to probe the details of the multiple processes occurring in filaments that can affect the properties of filament galaxies. Recently, Kim et al. (2016) identified seven filaments around the Virgo cluster, the nearest rich and dynamically young cluster (Aguerri et al. 2005), in which the majority of galaxies are faint ($M_B > -19$ mag; $\sim 88\%$ of the total sample) dwarfs. Therefore, Virgo filaments are prime targets for detailed investigations of the physical processes affecting galaxy properties in filament environment.

In response to this situation, in this work, we explored the impact of the filaments in the vicinity of the Virgo cluster on properties of filament galaxies using the photometric and spectroscopic data of the Sloan Digital Sky Survey (SDSS), Galaxy Evolution Explorer (GALEX) ultraviolet (UV) data, and neutral hydrogen (HI) gas data of the Arecibo Legacy Fast ALFA (ALFALFA) blind survey. In Section 2, we describe the basic data of galaxies in and around the Virgo filaments. Section 3 describes the selection of member galaxies in filaments. In Section 4, we show our results on the variations of galaxy properties (optical and UV colors, mass, central and global star formations, and HI gas content) as a function of the vertical filament distance. A discussion on physical processes in filaments is given in Section 5. Finally, we summarize our results in Section 6. Throughout this paper, we assume a $h = H_0/(100 \text{ km s}^{-1} \text{ Mpc}^{-1})$, the

matter density $\Omega_m = 0.27$, and the dark energy density $\Omega_\lambda = 0.73$ (Komatsu et al. 2011).

2. DATA

Our basic sample is drawn from galaxies at $z < 0.014$ in and around the Virgo filaments from the NASA-Sloan Atlas (NSA) catalog. In order to identify galaxies associated with galaxy groups residing on filaments, we make use of our sophisticated galaxy group catalog (Lee et al. in prep.). This is constructed for SDSS galaxies in the redshift range of $0.001 < z < 0.2$ with the use of the friends-of-friends for group detection. We examined the radial velocity distribution of NSA galaxies as a function of the group-centric distance. In this distribution, we overplotted a spherical symmetric infall model using measured velocity dispersion and virial radius of each group (Praton & Schneider 1994). We assigned NSA galaxies to group galaxies if they are bounded by the caustic curves of the infall model. Finally, we only selected galaxies that do not belong to groups in order to investigate how galaxies change their properties with varying distances from the filaments, avoiding contamination from member galaxies of groups located in filaments (e.g., Alpaslan et al. 2016; Bonjean et al. 2019). This allows studying the galaxy evolution in filament unaffected by local environmental effects occurring in groups (Robotham et al. 2013; Davies et al. 2015; Alpaslan et al. 2016).

Figure 1 shows the sky distribution of galaxies around the filaments. Gray dots indicate NSA galaxies at $z < 0.014$; different colored circles are the member galaxies belonging to different filaments (see Sec. 3), and red circles are the group galaxies. The spines of different filaments are plotted with different colored curves. The Crater filament galaxies are excluded from our analysis since the NSA catalog does not cover most of this filament in the southern hemisphere.

3. SELECTION OF MEMBER GALAXIES IN FILAMENTS

Since our study focuses on the properties of filament galaxies in the vertical direction from the filament spine, we need to define possible member galaxies belonging to each filament structure. In order to construct an accurate spatial distribution of galaxies in the NSA, we first converted the observed heliocentric radial velocities extracted from the NSA into velocities relative to the centroid of the Local Group using a method from Karachentsev & Makarov (1996). All NSA galaxies were then mapped in the supergalactic coordinate system (SGX, SGY, SGZ), which was converted from heliocentric radial velocities and positions (R.A. and Decl.) of

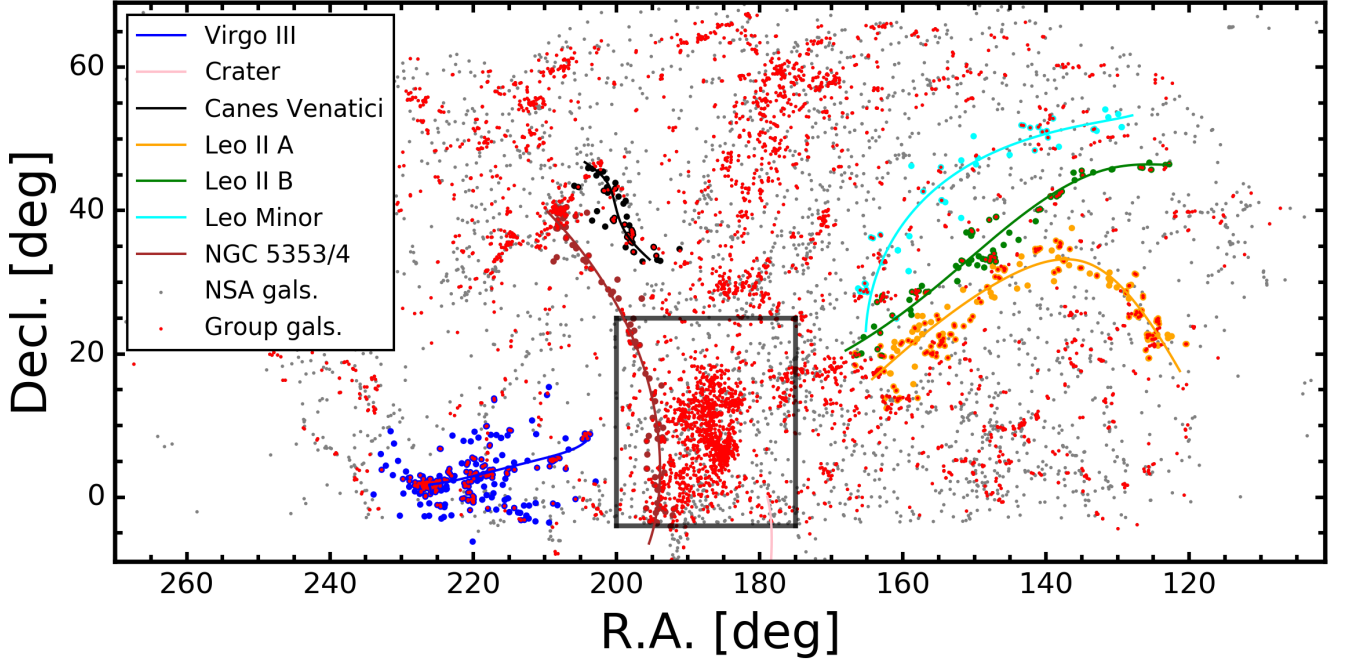


Figure 1. Spatial distribution of galaxies around the Virgo filaments in the equatorial coordinate system. Colored curves are spines of seven filaments identified by Kim et al. (2016) and colored circles are selected member galaxies that belong to the filaments. NSA galaxies at $z < 0.014$ and group galaxies are denoted as gray dots and red circles, respectively. The large rectangular box is the region of the Virgo cluster covered by the Extended Virgo Cluster Catalog (EVCC, Kim et al. 2014). In our study, we only consider galaxies that do not belong to galaxy groups (colored circles without red dots).

galaxies based on the assumption of a linear relationship between radial velocity and distance. We adopted the spines of filaments obtained by Kim et al. (2016) which are created by the three-dimensional third-order polynomial fitting of visually selected filament structures (see Kim et al. 2016 for details). We finally measured the three-dimensional vertical distances of galaxies (D_{ver}) from the filament spine in Mpc unit. In the case of Virgo III filament, since it is contiguous to the Virgo cluster in the SGZ direction, we rejected galaxies within a distance of $1.5 h^{-1}\text{Mpc}$ from the center of the supergalactic coordinate system in SGZ direction to avoid contamination from cluster galaxies.

Figure 2 presents galaxy number density (ρ_{gal}) profiles of each filament as a function of D_{ver} . We define ρ_{gal} at a D_{ver} as the number of galaxies over cylindrical volume along the filament spine in the supergalactic coordinate system. The ρ_{gal} was measured by the moving bin method with a bin size of $0.25 h^{-1}\text{Mpc}$ and a step size of $0.1 h^{-1}\text{Mpc}$ in D_{ver} direction. The overall feature in all filaments is that ρ_{gal} systematically decreases from the filament spine to a certain D_{ver} and then shows no variation with increasing D_{ver} . We have fitted decreasing part of the observed ρ_{gal} distribution with an

exponential function:

$$\rho_{\text{gal}} = \rho_0 \exp(-D_{\text{ver}}/R_s) \quad (1)$$

, where ρ_0 and R_s are central galaxy number density and scale length, respectively. The best-fit parameters are shown in Table 1 and the best-fit models are presented as red dashed lines in Figure 2. All R_s are found to be less than $1 h^{-1}\text{Mpc}$. Finally, we define member galaxies belonging to the filament as those within $3.5R_s$ from the filament spine. We note that the $3.5R_s$ well represents the location of a local minimum density in ρ_{gal} distribution (see red arrows for indicating $3.5R_s$ in Figure 2). The selected member galaxies in six filaments include a total of 289 galaxies.

For our analysis, we extracted photometric and spectroscopic parameters of member galaxies from the NSA; optical and UV magnitudes, stellar mass, and intensities of various emission lines (e.g., H α , H β , [OIII], [NII]). These parameters in the NSA are mainly derived from the SDSS optical data and with the addition of the GALEX UV data.

4. RESULTS

4.1. Stellar Mass Distribution and Color-Magnitude Diagram

Table 1. Properties of filaments

Name	ρ_0 [$h^{-3}\text{Mpc}^{-3}$]	R_s [$h^{-1}\text{Mpc}$]	Length [$h^{-1}\text{Mpc}$]	N
Virgo III	1.51 ± 0.21	0.90 ± 0.07	12.39	92
Canes Venatici	9.09 ± 2.45	0.25 ± 0.03	7.23	26
Leo II A	2.26 ± 0.42	0.45 ± 0.05	18.91	57
Leo II B	4.27 ± 1.04	0.29 ± 0.04	16.96	34
Leo Minor	16.31 ± 4.46	0.23 ± 0.03	5.91	26
NGC 5353/4	1.66 ± 0.31	0.51 ± 0.05	23.22	54

Notes. (1) Name of the filament

(2) Central galaxy number density of the exponential best-fit model

(3) Scale length of the exponential best-fit model

(4) Length of the filament in the SGX-SGY-SGZ plane

(5) Number of member galaxies that do not belong to groups

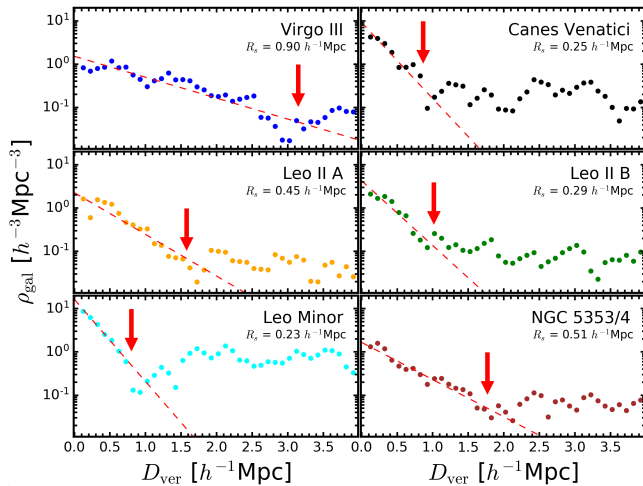


Figure 2. Galaxy number density profiles of six filaments as a function of the vertical distance from the filament spine (D_{ver}). Circles are observed number densities at different D_{ver} and dashed lines denote the best-fit exponential models. In each panel, scale length (R_s) of each filament is indicated and filament membership criterion (i.e., within $3.5R_s$ from the filament spine) is presented as a red arrow.

The filaments around the Virgo cluster defined by Kim et al. (2016) are the nearest large-scale structures from us ($\sim 14\text{--}41$ Mpc), mostly consisting of faint dwarf galaxies ($M_B > -19$; $\sim 88\%$ of the total sample). In Figure 3, we present the stellar mass (M_*) distribution of member galaxies in filaments. It is clear that most (87%) of our filament galaxies are lower mass ones with $\log h^2 M_*/M_\odot < 9$ in which median and standard deviation are 7.7 and 0.6, respectively.

We examined the photometric completeness of our galaxy sample by fitting the conventional Schechter function (see Equation 2 of Vulcani et al. 2013) to the stellar mass distribution of higher-mass galaxies with $\log h^2 M_*/M_\odot > 7.5$. We estimated the low-mass end

slope ($\alpha = -1.34$) and the characteristic stellar mass ($\log h^2 M_*/M_\odot = 10.47$) of the fitted mass function. Assuming this mass function is photometrically complete, we calculated the completeness of our filament galaxy sample at each mass bin which is the number ratio between the fitted Schechter function and observed stellar mass distribution. The completeness of galaxy samples for $\log h^2 M_*/M_\odot > 7$ and $\log h^2 M_*/M_\odot < 7$ are found to be 84% and 4%, respectively. We found that no significant change in our main results when we use only a relatively more complete sample with $\log h^2 M_*/M_\odot > 7$. We henceforth utilized the total sample galaxies without taking completeness into the consideration for our analysis.

Figure 4 shows the $g-r$ and near-ultraviolet ($NUV-r$) color-magnitude diagrams (CMDs) of galaxies in filaments (blue circles). For comparison with galaxies in a denser environment, we also overplot galaxies in the Virgo cluster (black dots) based on the SDSS optical and GALEX UV photometry of the EVCC catalog (Kim et al. 2014) adopting a distance modulus of the Virgo cluster of 31.1 (Mei et al. 2007). Further, we construct red sequences in the $g-r$ and $NUV-r$ CMDs by a linear least-square fitting to the early-type galaxies in the Virgo cluster (red solid lines in Figure 4). The filament galaxies show a blueward offset from the red sequence of the Virgo cluster in $g-r$; 80% (232/289) lie blueward of the -3σ deviation (red dashed line) from the Virgo red sequence in $g-r$. A more distinct offset is shown in the $NUV-r$ CMD owing to the longer baseline of $NUV-r$ color; 81% (234/289) of the filament galaxies lie blueward of the -3σ deviation (red dashed line) from the red sequence of the Virgo cluster. The $NUV-r$ CMD evidently shows that, at all magnitudes, the majority of filament galaxies occupy the region of the blue cloud as defined by galaxies in the local Universe

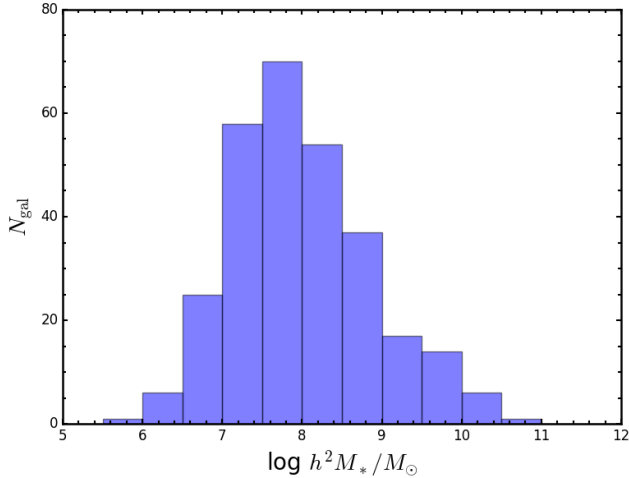


Figure 3. Stellar mass distribution of member galaxies in filaments.

(Wyder et al. 2007, blue curve). The $NUV - r$ CMD is particularly efficient to trace recent star-formation activity since the UV flux is sensitive to young (<1 Gyr) stellar populations. This indicates that the Virgo filaments are dominated by galaxies that have experienced recent star-formation.

4.2. Trends in Color and Stellar Mass

Gradients of color and stellar mass of galaxies are found in observed filaments consisting of massive galaxies with $>10^{10} M_\odot$; redder and more massive galaxies are closer to filaments, whereas the bluer and less massive galaxies are found further away from the filaments (e.g., Alpaslan et al. 2016; Malavasi et al. 2017; Kraljic et al. 2018; Bonjean et al. 2019; Luber et al. 2019; Sarron et al. 2019). It is intriguing to investigate whether low-mass dwarf galaxies in filaments also follow this trend.

We examined color and stellar mass distributions of filament galaxies as a function of the scaled vertical distance from the filament spine (D_{ver}/R_s) which is defined as D_{ver} divided by the measured R_s of the filament. Further, we calculated mean color and mean mass along the D_{ver}/R_s using the moving bin method, where bin size and step size of the D_{ver}/R_s are 1 and 0.4, respectively. The errors of color and mass of each bin are calculated by the bootstrap resampling method.

Figure 5 illustrates $g - r$ color (top) and stellar mass (bottom) distributions as a function of the D_{ver}/R_s . It appears that color and stellar mass correlate with the vertical distance from the filament spine; that is, $g - r$ color becomes blue and stellar mass decreases with increasing D_{ver}/R_s . We performed a Kolmogorov-Smirnov (K-S) test to quantify the statistical significance of this trend. We divided galaxies into two sub-

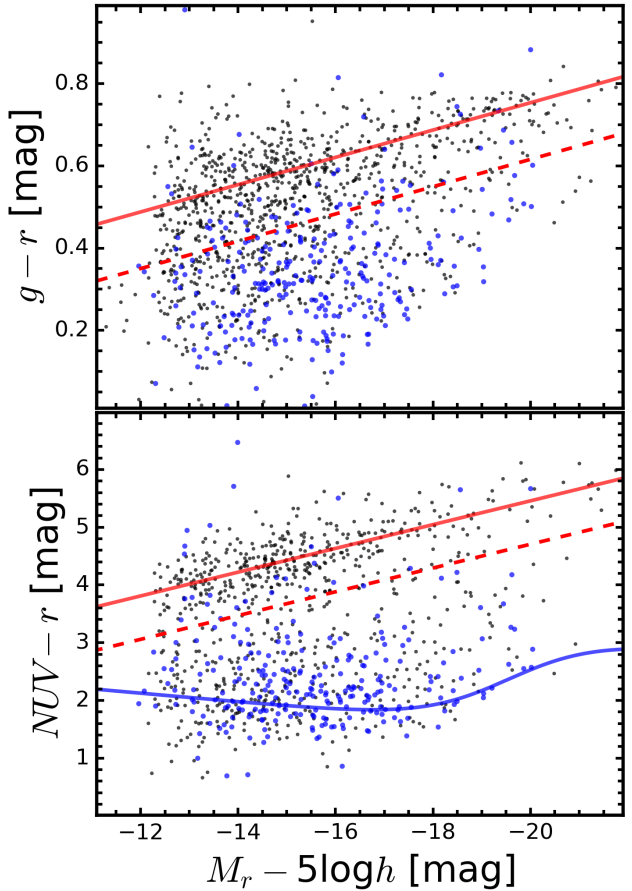


Figure 4. $g - r$ (top) and $NUV - r$ (bottom) color-magnitude diagrams of galaxies in filaments (blue circles). For comparison, galaxies in the Virgo cluster are also overplotted (black dots). The red solid lines represent the red sequence of the Virgo cluster and the red dashed lines are -3σ deviation from the red sequence. In the $NUV - r$ CMD, the blue curve indicates the blue cloud defined by Wyder et al. (2007).

samples located in the inner ($0 \leq D_{\text{ver}}/R_s \leq 1.75$) and outer ($1.75 < D_{\text{ver}}/R_s \leq 3.5$) regions of the filament. The test between two subsamples provides probabilities of 0.0312 and 0.0126 for color and stellar mass, respectively, rejecting that the color and stellar mass distributions between two subsamples are drawn from the same parent one. This implies that negative gradients of color and stellar mass are evident in filaments mostly consisting of low-mass ($<10^9 M_\odot$) dwarf galaxies. Combining with previous results mainly based on more massive galaxies, it can be said that the color and stellar mass gradients are generally observed in the vertical direction of filaments regardless of mass range.

We divided filament galaxies into higher-mass ($\log h^2 M_*/M_\odot > 8$) and lower-mass ($\log h^2 M_*/M_\odot \leq 8$) subsamples where $\log h^2 M_*/M_\odot = 8$ is a median stellar mass of

filament galaxies. Figure 6 shows $g - r$ color and stellar mass distributions of higher-mass (circles and dashed line) and lower-mass (squares and solid line) galaxies as a function of the D_{ver}/R_s . The most notable feature is that the color distribution of higher-mass galaxies appears to be different from that of lower-mass galaxies (see top panel of Figure 6); higher-mass galaxies show a rather flat distribution, whereas the color of lower-mass galaxies appears to decrease with the D_{ver}/R_s . The K-S tests of higher- and lower-mass galaxies yield probabilities of 0.8137 and 0.0450, respectively, for color distributions between the inner ($0 \leq D_{\text{ver}}/R_s \leq 1.75$) and outer ($1.75 < D_{\text{ver}}/R_s \leq 3.5$) regions of the filament. This indicates no statistically significant difference in the color distributions of high mass-galaxies between the inner and outer regions of the filament. On the other hand, the color distribution of lower-mass galaxies closer to the filament spine shows a statistically significant difference from that of counterparts far from the filament.

In the case of stellar mass distributions, both of the two subsamples in different mass ranges do not show a significant variation of stellar mass with the D_{ver}/R_s (see bottom panel of Figure 6). The K-S tests of higher- and lower-mass galaxies yield probabilities of 0.3187 and 0.3314, respectively, for stellar mass distributions between the inner ($0 \leq D_{\text{ver}}/R_s \leq 1.75$) and outer ($1.75 < D_{\text{ver}}/R_s \leq 3.5$) regions of the filament. This indicates that the stellar mass gradients of two subsamples are not statistically significant.

4.3. Star-forming Galaxies in Filaments

Star-forming galaxies are mostly found in less dense environments such as field and filament (Haines et al. 2007; Gavazzi et al. 2010). They are attractive objects for inspecting the degree of environmental effects in terms of their strengths of star-formation. In this regard, investigation of the star-formation activity of star-forming galaxies at different vertical distances from the filament spine will enable us to understand the environment of filament.

We selected star-forming galaxies using the Baldwin-Phillips-Terlevich (BPT) emission line diagnostic diagram (Baldwin et al. 1981) that allows discriminating star-forming galaxies from possible active galactic nuclei (AGNs). Figure 7 is the BPT diagram where the emission-line ratios $[\text{OIII}]/\text{H}\beta$ and $[\text{NII}]/\text{H}\alpha$ extracted from the NSA are used. We define star-forming galaxies which locate below the empirical demarcation line of Kauffmann et al. (2003, red curve). Only galaxies with strong $\text{H}\alpha$ equivalent width (EW) (i.e., $\text{EW}(\text{H}\alpha) > 2 \text{ \AA}$) are also considered, and finally, 161 star-forming galax-

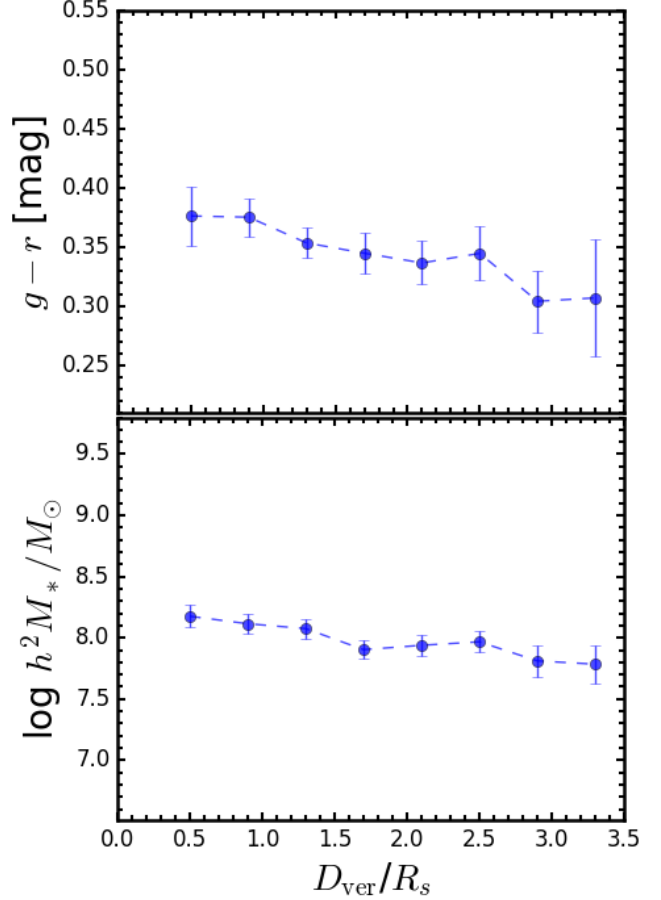


Figure 5. $g - r$ color (top) and stellar mass (bottom) versus scaled vertical distance from the filament spine (D_{ver}/R_s). The error bar of each bin indicates bootstrap resampling uncertainty.

ies are identified. AGNs are located above the theoretical starburst model line of Kewley et al. (2001, black curve).

The $\text{H}\alpha$ emission traces the ongoing star-formation activity from massive stars with timescales of a few tens of Myr. Figure 8 shows $\text{EW}(\text{H}\alpha)$ distributions of higher-mass ($\log h^2 M_*/M_\odot > 8$, top panel) and lower-mass ($\log h^2 M_*/M_\odot \leq 8$, bottom panel) galaxies as a function of the D_{ver}/R_s . The $\text{EW}(\text{H}\alpha)$ distributions between two subsamples appear to be different; the $\text{EW}(\text{H}\alpha)$ values of higher-mass galaxies likely decrease with the D_{ver}/R_s , but lower-mass galaxies show no distinct trend of $\text{EW}(\text{H}\alpha)$. The K-S tests of higher- and lower-mass galaxies yield probabilities of 0.0094 and 0.5685, respectively, for $\text{EW}(\text{H}\alpha)$ distributions between the inner ($0 \leq D_{\text{ver}}/R_s \leq 1.75$) and outer ($1.75 < D_{\text{ver}}/R_s \leq 3.5$) regions of the filament. This indicates that a possible $\text{EW}(\text{H}\alpha)$ gradient from the filament spine is only seen for the higher-mass galaxies. We note that $\text{EW}(\text{H}\alpha)$ value

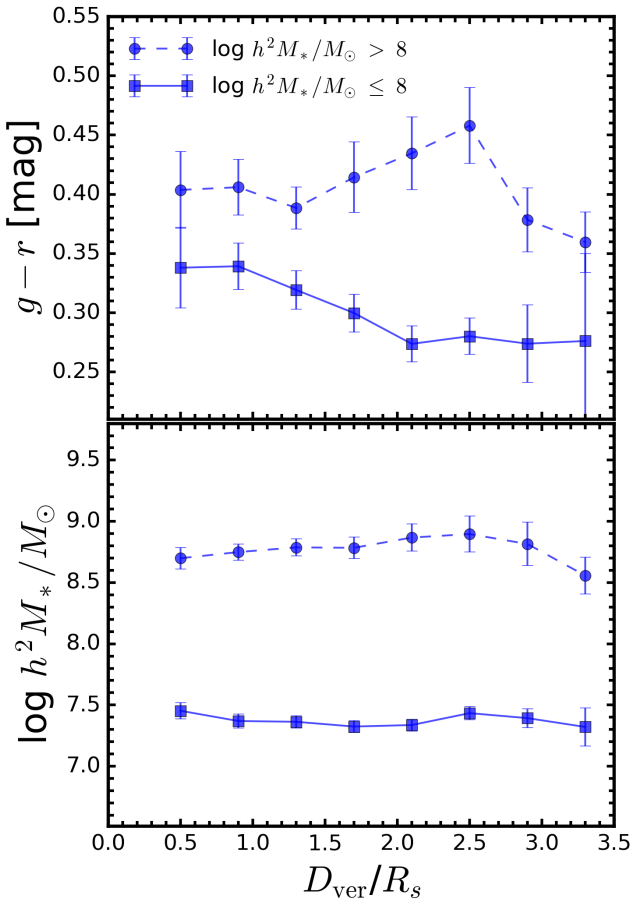


Figure 6. $g-r$ color (top) and stellar mass (bottom) versus scaled vertical distance from the filament spine (D_{ver}/R_s) for galaxies in different mass ranges. The circles and dashed lines represent higher-mass ($\log h^2 M_*/M_\odot > 8$) galaxies and the squares and solid lines are lower-mass ($\log h^2 M_*/M_\odot \leq 8$) galaxies. The error bar of each bin indicates bootstrap resampling uncertainty.

from the NSA generally provides information on the central region of a galaxy due to the 3 arcsec (i.e., 204–596 pc at a distance range of 14–41 Mpc for our filaments) fiber aperture of the SDSS spectroscopic observations. Therefore, current star-formation in the central region of higher-mass galaxies is more active for those located closer to the filament spine.

On the other hand, the global star-formation of the entire region of a galaxy can be examined by UV photometry. Figure 9 shows $NUV - r$ color distributions of higher-mass ($\log h^2 M_*/M_\odot > 8$, top panel) and lower-mass ($\log h^2 M_*/M_\odot \leq 8$, bottom panel) galaxies as a function of the D_{ver}/R_s . The $NUV - r$ color distribution of higher-mass galaxies is likely to show a trend with the D_{ver}/R_s ; $NUV - r$ color very smoothly increases with the D_{ver}/R_s . On the other hand, the $NUV - r$ colors of lower-mass galaxies appear to de-

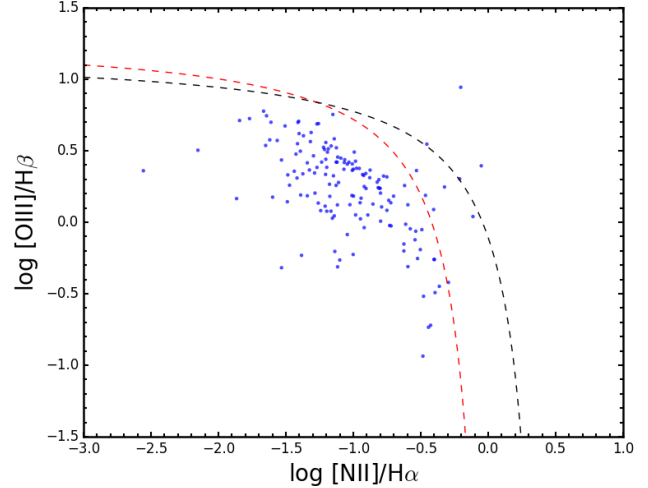


Figure 7. BPT diagram of filament galaxies. Star-forming galaxies are defined as those below the red curve of Kauffmann et al. (2003). AGNs are those above the black curve of Kewley et al. (2001).

crease with the D_{ver}/R_s . However, the K-S tests of higher- and lower-mass galaxies yield probabilities of 0.0904 and 0.0387, respectively, for $NUV - r$ color distributions between the inner ($0 \leq D_{\text{ver}}/R_s \leq 1.75$) and outer ($1.75 < D_{\text{ver}}/R_s \leq 3.5$) regions of the filament, indicating that $NUV - r$ color gradient is statistically significant only for lower-mass galaxies. This implies that recent (< 1 Gyr), global star-formation of lower-mass galaxies residing closer to the filament is less active than counterparts with large displacement from the filament spine.

4.4. HI Content of Filament Galaxies

HI gas content within a galaxy has been a good tracer of different environmental effects in a cluster environment (e.g., Boselli & Gavazzi 2006). In terms of the role of the filament environment in regulating the evolution of galaxies, we also investigate the HI gas content of galaxies residing on our filaments using data from the ALFALFA (Haynes et al. 2018) blind survey. The flux limit of the ALFALFA corresponds to the detection limit of the HI mass $M_{\text{HI}} = 10^{7.4} M_\odot$ at the distance of the Virgo cluster (Haynes et al. 2011, 2018). We note that owing to proximity to us, Virgo filaments are optimal for the detection of HI gas in faint, low mass galaxies. Of our 289 filament galaxies, 184 are included in the sky coverage of the ALFALFA survey (Haynes et al. 2018, see dashed contour in Figure 10), which covers the area around the Virgo cluster at declinations 0° – 37° . We found that HI gas of 69% (i.e., 127 galaxies) of the galaxies are detected and HI gas masses of galaxies are also

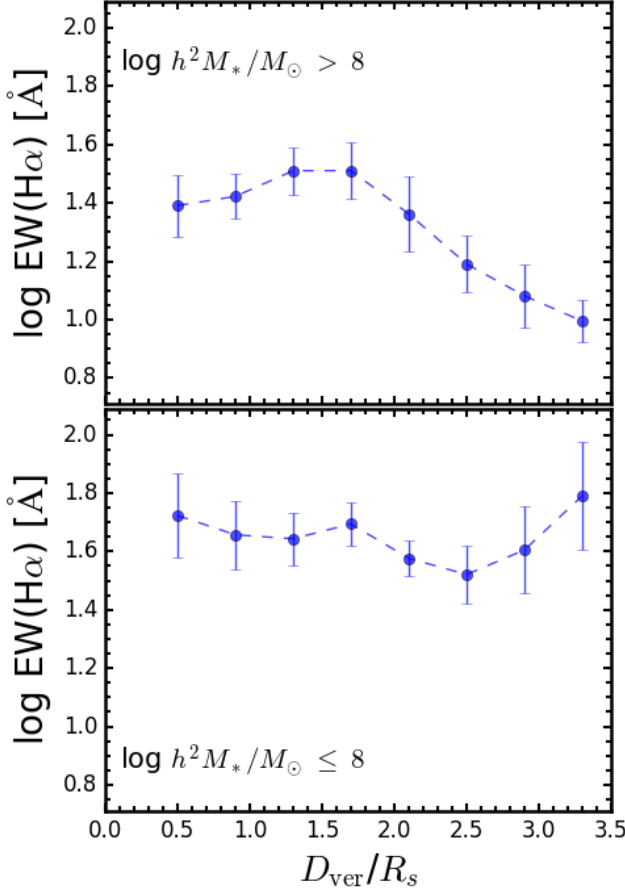


Figure 8. Equivalent width of H α emission line (EW(H α)) versus scaled vertical distance (D_{ver}/R_s) from the filament spine of higher-mass ($\log h^2 M_*/M_\odot > 8$) galaxies (top) and lower-mass ($\log h^2 M_*/M_\odot \leq 8$) galaxies (bottom). The error bar of each bin indicates bootstrap resampling uncertainty.

extracted from the ALFALFA data. Figure 10 shows the sky distribution of HI detected galaxies (crosses).

Figure 11 shows the HI fraction (f_{HI}) distributions of higher-mass ($\log h^2 M_*/M_\odot > 8$, top panel) and lower-mass ($\log h^2 M_*/M_\odot \leq 8$, bottom panel) galaxies as a function of the D_{ver}/R_s , where the HI fraction is defined as the ratio between HI gas mass (M_{HI}) and stellar mass (M_*):

$$f_{\text{HI}} = \log \frac{M_{\text{HI}}}{M_*}. \quad (2)$$

At a given D_{ver}/R_s , lower-mass galaxies are systematically higher f_{HI} than higher-mass ones. This is consistent with the general relationship between f_{HI} and stellar mass found in the Virgo cluster, in which the average gas fraction increases with decreasing stellar mass (see Figure 5 of Hallenbeck et al. 2012).

The f_{HI} distribution of higher-mass galaxies is likely to show a trend with the D_{ver}/R_s ; f_{HI} decreases with

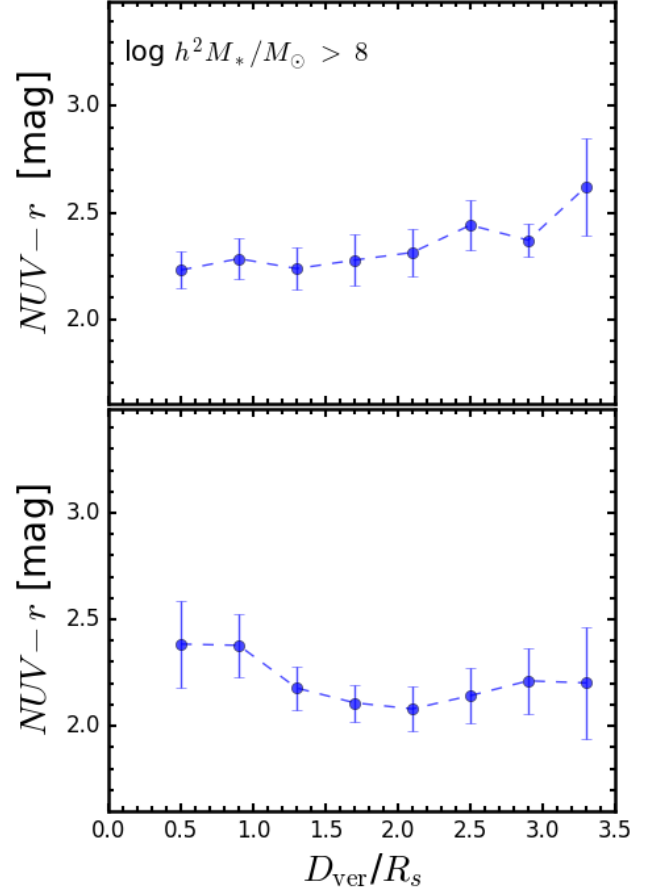


Figure 9. $NUV - r$ color versus scaled vertical distance (D_{ver}/R_s) from the filament spine of higher-mass ($\log h^2 M_*/M_\odot > 8$) galaxies (top) and lower-mass ($\log h^2 M_*/M_\odot \leq 8$) galaxies (bottom). The error bar of each bin indicates bootstrap resampling uncertainty.

increasing vertical distance from the filament spine. Lower-mass galaxies also appear to show a hint of a very smooth increase of f_{HI} with the D_{ver}/R_s . However, the K-S tests of higher- and lower-mass galaxies yield probabilities of 0.2426 and 0.4351, respectively, for f_{HI} distributions between the inner ($0 \leq D_{\text{ver}}/R_s \leq 1.75$) and outer ($1.75 < D_{\text{ver}}/R_s \leq 3.5$) regions of the filament, indicating that f_{HI} gradients of both two subsamples are not statistically significant.

5. DISCUSSION

In the filament structures around the Virgo cluster which are mostly composed of faint, low mass ($\log h^2 M_*/M_\odot < 9$) galaxies, we observe negative stellar mass and $g - r$ color gradients (see Figure 5). These features are also shown in previous results based on the sample of massive galaxies in more distant filaments (Mahajan et al. 2018; Luber et al. 2019; Sarron et al. 2019); galaxies closer to the filament spine

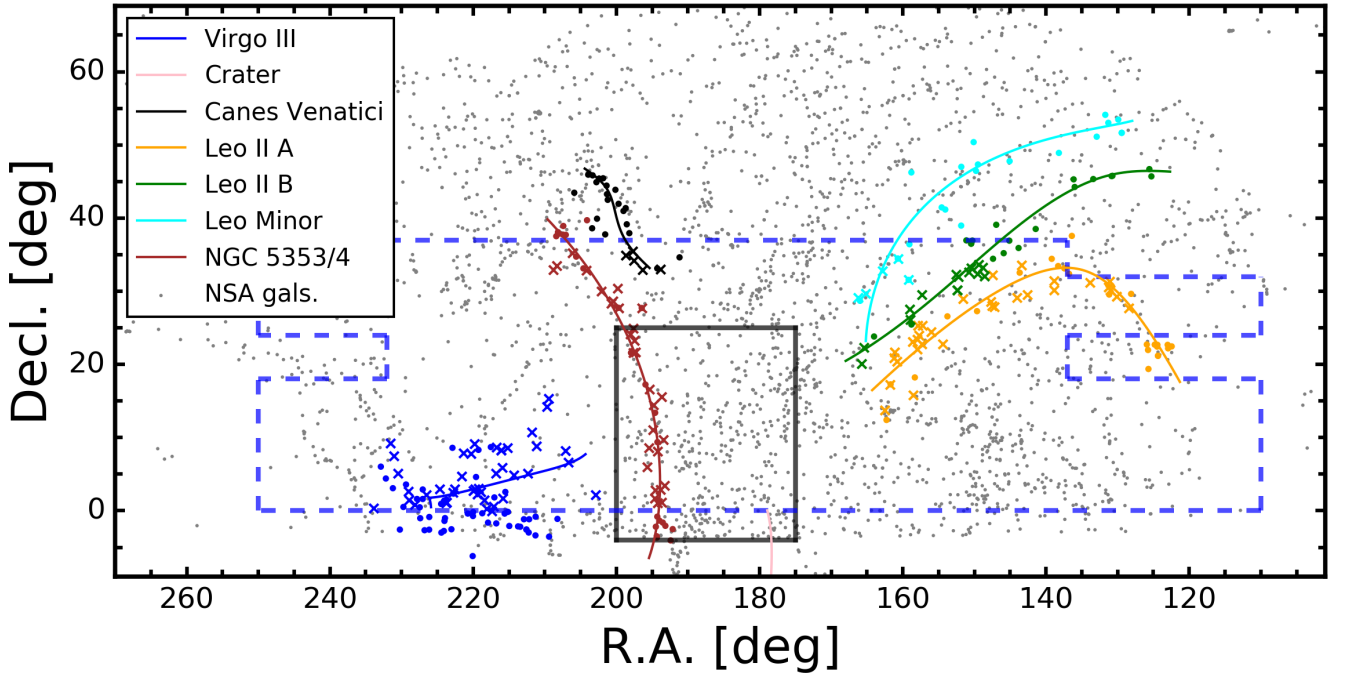


Figure 10. Spatial distribution of filament galaxies with HI detection from the ALFALFA survey data (colored crosses). Colored circles denote filament galaxies with HI non-detection. Gray circles are NSA galaxies not associated with the filaments and the galaxy groups. The large rectangular box is the region of the EVCC. The coverage of the ALFALFA survey is presented by the blue dashed contour.

have higher stellar masses and redder colors than those showing large displacement from filaments. A generally suggested mechanism for this mass gradient is galaxy mergers in the past (Malavasi et al. 2017; Kraljic et al. 2018), in which more massive galaxies finish their assembly of stellar mass closer to the filament spine owing to a higher merger rate (Dubois et al. 2014). The formation of these massive merger remnants is accompanied by subsequent changes in their colors since the mass regulates properties of galaxies (Peng et al. 2010). This is in line with the suggestion that mass is the main parameter driving galaxy properties in filaments (e.g., Robotham et al. 2013; Alpaslan et al. 2015, 2016).

Interestingly, when we narrow down the mass ranges of galaxies by dividing into two subsamples (i.e., higher-mass with $\log h^2 M_*/M_\odot > 8$ and lower-mass with $\log h^2 M_*/M_\odot \leq 8$), mass gradients are not observed for both mass ranges (see bottom panel of Figure 6). In this case, color gradients are also not anticipated in terms of the connection between stellar mass and color of galaxies. This is shown for higher-mass galaxies; stellar mass and color of higher-mass galaxies are almost statistically invariant with the vertical distance from the filament spine. However, in the case of lower-mass galaxies, the overall feature of the color distribution is decoupled from the stellar mass distribution; although stellar masses of galaxies are similar for all distances,

the negative color gradient is clearly displayed (see top panel of Figure 6). This indicates that an additional process might be responsible for the color gradient shown in lower-mass galaxies.

The local environment is generally considered as the second parameter in determining galaxy properties at fixed stellar mass (e.g., Peng et al. 2010; Geha et al. 2012; Wetzel et al. 2012). In this regard, the interaction between galaxies is thought to be one of the typical environmental processes. The strong tidal forces in interacting galaxies can remove a large amount of gas from the outer part of galaxies, leading to a subsequent decrease in global star-formation activity (Barnes & Hernquist 1991; Mihos & Hernquist 1994, 1996; Di Matteo et al. 2007). Meanwhile, galaxy interaction also causes funneling gas into the central region of galaxies, which could trigger strong central bursts of star-formation (Barnes & Hernquist 1996; Mihos & Hernquist 1996; Kewley et al. 2006).

The $NUV - r$ color distribution of lower-mass galaxies shows a clear negative correlation with the distance from the filament spine (see Figure 9), indicating global star-formation is depressed for lower-mass galaxies residing toward the filament spine. This is consistent with a general prediction that the efficiency of galaxy interaction could decrease moving further away from the filament spine. However, contrary to an expectation of gas

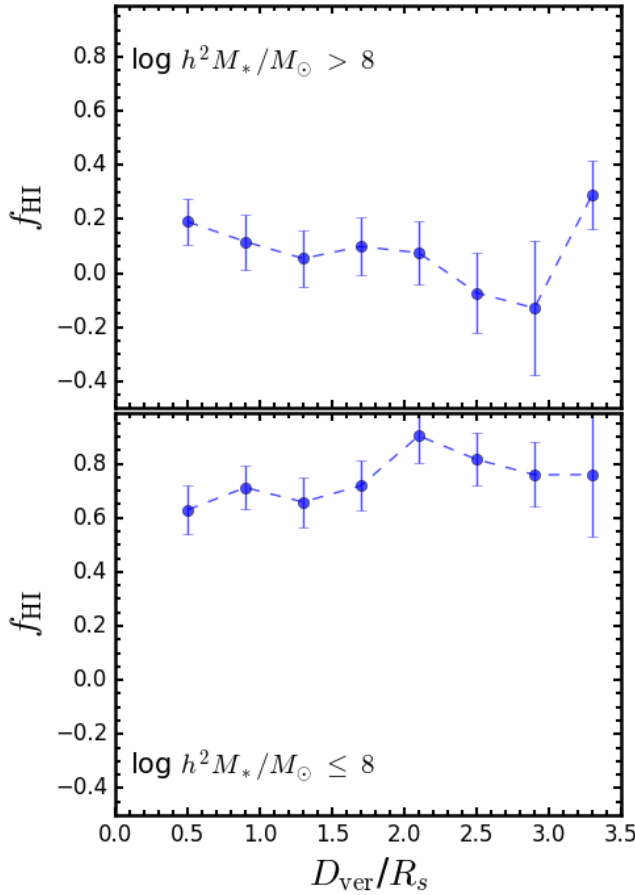


Figure 11. HI gas fraction (f_{HI}) versus scaled vertical distance (D_{ver}/R_s) from the filament spine of higher-mass ($\log h^2 M_*/M_\odot > 8$) galaxies (top) and lower-mass ($\log h^2 M_*/M_\odot \leq 8$) galaxies (bottom). The error bar of each bin indicates bootstrap resampling uncertainty.

flows toward the central region by galaxy interaction, lower-mass galaxies show no distinct variation of central star-formation, traced by $EW(H\alpha)$, with the distance from the filament spine (see Figure 8); i.e., lower-mass galaxies at closer to the spine do not show enhanced central star-formation. The restoring force of a lower-mass galaxy on possessing interstellar medium could be very small due to its shallow potential well. If the tidal force exerted by a companion galaxy is greater than the restoring force of the lower-mass galaxy, a large fraction of its gaseous material would be perturbed and then removed. Therefore, the $EW(H\alpha)$ distribution of lower-mass galaxies could be explained by a lack of available fuel infalling from the outskirts of galaxies for their central star-formation.

In the case of higher-mass galaxies with deep potential wells, much of the original gas reservoir is likely to be retained against the tidal force by the interaction.

Our result clearly indicates that global star-formation of higher-mass galaxies is not sensitive to the galaxies' distance from the filament spine (see Figure 9). In this case, on the other hand, higher-mass galaxies residing closer to the filament spine would show an enhancement in central star-formation by funneling a large quantity of available gas into the central region of the galaxies (see Figure 8).

The environmental mechanism related to the intergalactic medium such as ram-pressure stripping is important for regulating star-formation and the evolution of galaxies in galaxy clusters (e.g., Gunn & Gott 1972; Larson et al. 1980). Benítez-Llambay et al. (2013) also show that hydrodynamical interaction between a galaxy and intergalactic gas in the filaments results in the removal of much of the gaseous component within a galaxy when the galaxy traverses the filaments. Therefore, ram-pressure stripping in the filament, the so-called “cosmic-web stripping” (Benítez-Llambay et al. 2013), is also expected to potentially influence on galaxy properties in the filament environment (Sancisi et al. 2008; Aragon Calvo et al. 2019). Numerical simulations and X-ray observations might support this idea such that filaments host warm-hot intergalactic medium (WHIM) as the dominant baryon mass contribution in filaments (e.g., Eckert et al. 2015; Akamatsu et al. 2017; Parekh et al. 2017; Martizzi et al. 2019; Tanimura et al. 2019).

The ram-pressure stripping can be probed by the HI cold gas content within galaxies. In this regard, Luber et al. (2019) found a positive HI fraction gradient of galaxies with a mean stellar mass of $10^{10} M_\odot$ in which galaxies further away from the filaments show a higher HI fraction, indicating that HI gas in galaxies closer to filaments can be efficiently removed by process related to the intrafilament medium. The deprivation of gas in galaxies would be more pronounced in low-mass galaxies due to their shallower potential wells. However, in the case of our lower-mass ($\log h^2 M_*/M_\odot \leq 8$) subsample, the difference of HI fraction distributions between the inner and outer regions of the filament is not statistically significant (see Figure 11). This implies that the ram-pressure stripping does not play a significant role in reducing HI gas of lower-mass galaxies in filaments. It might be tempting to ascribe the lack of distinct HI fraction gradient of filament galaxies to the intrinsic property of intergalactic medium in the Virgo filaments characterized by a low density of WHIM.

In terms of understanding galaxy evolution in filaments, it can be said that galaxies can replenish HI gas content through cold mode gas accretion from the filaments (Kereš et al. 2005 and references therein; Kleiner et al. 2017). This is supported by numerical simulations

which also show that filaments host diffuse HI gas at low redshift (e.g., [Popescu et al. 2009](#)). [Kleiner et al. \(2017\)](#) found tentative evidence of cold gas accretion for massive galaxies with stellar masses of $>10^{11} M_{\odot}$ from the intrafilament medium, whereas a hint of gas accretion was not observed for low-mass galaxies with $<10^{11} M_{\odot}$. They proposed that cold mode gas accretion is only allowed for the most massive galaxies in filaments owing to larger gravitational potentials of galaxies enough to pull cold gas from the intrafilament medium. The difference in HI fraction of our higher-mass galaxies between the inner and outer regions of the filament is not found to be statistically significant (see Figure 11), indicating the absence of any gas accretion. Our result is in line with that of [Kleiner et al. \(2017\)](#), considering that the mass range of our higher-mass galaxies ($\log h^2 M_{*}/M_{\odot} \sim 8-11$) corresponds to that of their low-mass galaxies.

6. SUMMARY AND CONCLUSIONS

In this study, we have explored properties of galaxies in six filaments around the Virgo cluster, which are the nearest large-scale structures from us ($\sim 14-41$ Mpc), as a function of the vertical distance from the filament spine. Using the NSA and galaxy group catalogs, we selected galaxies that do not belong to galaxy groups in filaments and defined filament member galaxies that are located within 3.5 scale length from the filament spine. The main results are the following:

- (i) The filaments are mainly composed of low-mass dwarf galaxies; the median value of the stellar mass distribution is $\log h^2 M_{*}/M_{\odot} = 7.7$ and 87% of the total sample have stellar mass with $\log h^2 M_{*}/M_{\odot} < 9$. In $g - r$ and $NUV - r$ CMDs, the filament galaxies show a blueward offset from the red sequence of the Virgo cluster and are dominantly located on the blue cloud.
- (ii) We observe that $g - r$ color and stellar mass correlate with the vertical distance from the filament spine; color becomes blue and stellar mass decreases with increasing vertical filament distance. We confirm that these trends are statistically significant in the K-S test between two subsamples located in the inner and outer regions of the filament. We propose that the negative color and stellar mass gradients of galaxies found in our filaments can be explained by mass assembly depending on efficiency of galaxy mergers at different vertical distances from the filament spine and subsequent change in their colors regulated by final mass.

- (iii) We also examined the $g - r$ color and stellar mass distributions of galaxy subsamples in different mass ranges; higher-mass galaxies with $\log h^2 M_{*}/M_{\odot} > 8$ and lower-mass galaxies with $\log h^2 M_{*}/M_{\odot} \leq 8$. The $g - r$ color distribution of higher-mass galaxies is found to be different from that of lower-mass galaxies; higher-mass galaxies have a flat distribution against the vertical filament distance, whereas lower-mass galaxies show a clear negative color gradient. In the case of stellar mass distribution, a significant trend of stellar mass with the vertical filament distance is not shown for both subsamples in different mass ranges.
- (iv) We inspected $EW(H\alpha)$ and $NUV - r$ color distributions of higher- and lower-mass subsamples, which trace central and global star-formation activities of galaxies, respectively, using star-forming galaxies selected by the BPT emission line diagnostic diagram. The $EW(H\alpha)$ distributions between two subsamples are different; we observe a negative $EW(H\alpha)$ gradient for higher-mass galaxies, whereas lower-mass galaxies show no distinct variation of $EW(H\alpha)$. On the other hand, $NUV - r$ color distributions exhibit counter-trend in different mass-ranges; the $NUV - r$ color distribution of higher-mass galaxies shows no statistically strong dependence on the vertical filament distance, but lower-mass galaxies show a distinct negative $NUV - r$ color gradient. All the observed $EW(H\alpha)$ and $NUV - r$ color distributions of higher- and lower-mass subsamples can be qualitatively explained by different star-formation efficiency in galaxy interactions depending on masses of galaxies.
- (v) We observe no clear trend in the distributions of HI fraction for two subsamples detected from the ALFALFA blind survey data. Both higher- and lower-mass galaxies show no statistically significant variations in HI fractions with the vertical filament distance. This indicates that possible mechanisms related to intrafilament medium, such as ram-pressure stripping and gas accretion, could be ignorable for galaxies in the Virgo filaments. Although the ALFALFA data obtained from Arecibo single-dish telescope provides us a statistical view of the gas content of galaxies, further deep HI surveys using more sensitive very-large array telescopes will improve our understanding of the HI content of galaxies within the Virgo filaments.

We are grateful to the anonymous referee for helpful comments and suggestions that improved the clarity and quality of this paper. Y.D.L, acting as the corresponding author, acknowledges support from Basic Science Research Program through the National Research Foundation of Korea (NRF) funded by the Ministry of Education (2020R1A6A3A01099777). S.C.R., acting as the corresponding author, acknowledges support from the Basic Science Research Program through the National Research Foundation of Korea (NRF) funded by the

Ministry of Education (2018R1A2B2006445). Support for this work was also provided by the NRF to the Center for Galaxy Evolution Research (2017R1A5A1070354). S.K. acknowledges support from the Basic Science Research Program through the National Research Foundation of Korea (NRF) funded by the Research Staff Program (NRF-2019R1I1A1A01061237). We would like to thank Editage (www.editage.co.kr) for English language editing.

REFERENCES

Aguerri, J. A. L., Gerhard, O. E., Arnaboldi, M., et al. 2005, AJ, 129, 2585, doi: [10.1086/429936](https://doi.org/10.1086/429936)

Akamatsu, H., Fujita, Y., Akahori, T., et al. 2017, A&A, 606, A1, doi: [10.1051/0004-6361/201730497](https://doi.org/10.1051/0004-6361/201730497)

Alpaslan, M., Driver, S., Robotham, A. S. G., et al. 2015, MNRAS, 451, 3249, doi: [10.1093/mnras/stv1176](https://doi.org/10.1093/mnras/stv1176)

Alpaslan, M., Grootes, M., Marcum, P. M., et al. 2016, MNRAS, 457, 2287, doi: [10.1093/mnras/stw134](https://doi.org/10.1093/mnras/stw134)

Aragon Calvo, M. A., Neyrinck, M. C., & Silk, J. 2019, The Open Journal of Astrophysics, 2, 7, doi: [10.21105/astro.1607.07881](https://doi.org/10.21105/astro.1607.07881)

Baldwin, J. A., Phillips, M. M., & Terlevich, R. 1981, PASP, 93, 5, doi: [10.1086/130766](https://doi.org/10.1086/130766)

Barnes, J. E., & Hernquist, L. 1996, ApJ, 471, 115, doi: [10.1086/177957](https://doi.org/10.1086/177957)

Barnes, J. E., & Hernquist, L. E. 1991, ApJL, 370, L65, doi: [10.1086/185978](https://doi.org/10.1086/185978)

Benítez-Llambay, A., Navarro, J. F., Abadi, M. G., et al. 2013, ApJL, 763, L41, doi: [10.1088/2041-8205/763/2/L41](https://doi.org/10.1088/2041-8205/763/2/L41)

Bond, J. R., Kofman, L., & Pogosyan, D. 1996, Nature, 380, 603, doi: [10.1038/380603a0](https://doi.org/10.1038/380603a0)

Bonjean, V., Aghanim, N., Douspis, M., Malavasi, N., & Tanimura, H. 2019, arXiv e-prints, arXiv:1912.06559. <https://arxiv.org/abs/1912.06559>

Boselli, A., & Gavazzi, G. 2006, PASP, 118, 517, doi: [10.1086/500691](https://doi.org/10.1086/500691)

Chen, Y.-C., Ho, S., Mandelbaum, R., et al. 2017, MNRAS, 466, 1880, doi: [10.1093/mnras/stw3127](https://doi.org/10.1093/mnras/stw3127)

Cybulski, R., Yun, M. S., Fazio, G. G., & Gutermuth, R. A. 2014, MNRAS, 439, 3564, doi: [10.1093/mnras/stu200](https://doi.org/10.1093/mnras/stu200)

Darvish, B., Mobasher, B., Sobral, D., et al. 2015, ApJ, 814, 84, doi: [10.1088/0004-637X/814/2/84](https://doi.org/10.1088/0004-637X/814/2/84)

Davies, L. J. M., Robotham, A. S. G., Driver, S. P., et al. 2015, MNRAS, 452, 616, doi: [10.1093/mnras/stv1241](https://doi.org/10.1093/mnras/stv1241)

De Lucia, G., Weinmann, S., Poggianti, B. M., Aragón-Salamanca, A., & Zaritsky, D. 2012, MNRAS, 423, 1277, doi: [10.1111/j.1365-2966.2012.20983.x](https://doi.org/10.1111/j.1365-2966.2012.20983.x)

Di Matteo, P., Combes, F., Melchior, A. L., & Semelin, B. 2007, A&A, 468, 61, doi: [10.1051/0004-6361:20066959](https://doi.org/10.1051/0004-6361:20066959)

Dubois, Y., Pichon, C., Welker, C., et al. 2014, MNRAS, 444, 1453, doi: [10.1093/mnras/stu1227](https://doi.org/10.1093/mnras/stu1227)

Eckert, D., Jauzac, M., Shan, H., et al. 2015, Nature, 528, 105, doi: [10.1038/nature16058](https://doi.org/10.1038/nature16058)

Fujita, Y. 2004, PASJ, 56, 29, doi: [10.1093/pasj/56.1.29](https://doi.org/10.1093/pasj/56.1.29)

Gavazzi, G., Fumagalli, M., Cucciati, O., & Boselli, A. 2010, A&A, 517, A73, doi: [10.1051/0004-6361/201014153](https://doi.org/10.1051/0004-6361/201014153)

Geha, M., Blanton, M. R., Yan, R., & Tinker, J. L. 2012, ApJ, 757, 85, doi: [10.1088/0004-637X/757/1/85](https://doi.org/10.1088/0004-637X/757/1/85)

Gunn, J. E., & Gott, III, J. R. 1972, ApJ, 176, 1, doi: [10.1086/151605](https://doi.org/10.1086/151605)

Haines, C. P., Gargiulo, A., La Barbera, F., et al. 2007, MNRAS, 381, 7, doi: [10.1111/j.1365-2966.2007.12189.x](https://doi.org/10.1111/j.1365-2966.2007.12189.x)

Hallenbeck, G., Papastergis, E., Huang, S., et al. 2012, AJ, 144, 87, doi: [10.1088/0004-6256/144/3/87](https://doi.org/10.1088/0004-6256/144/3/87)

Haynes, M. P., Giovanelli, R., Martin, A. M., et al. 2011, AJ, 142, 170, doi: [10.1088/0004-6256/142/5/170](https://doi.org/10.1088/0004-6256/142/5/170)

Haynes, M. P., Giovanelli, R., Kent, B. R., et al. 2018, ApJ, 861, 49, doi: [10.3847/1538-4357/aac956](https://doi.org/10.3847/1538-4357/aac956)

Karachentsev, I. D., & Makarov, D. A. 1996, AJ, 111, 794, doi: [10.1086/117825](https://doi.org/10.1086/117825)

Kauffmann, G., Heckman, T. M., Tremonti, C., et al. 2003, MNRAS, 346, 1055, doi: [10.1111/j.1365-2966.2003.07154.x](https://doi.org/10.1111/j.1365-2966.2003.07154.x)

Kereš, D., Katz, N., Weinberg, D. H., & Davé, R. 2005, MNRAS, 363, 2, doi: [10.1111/j.1365-2966.2005.09451.x](https://doi.org/10.1111/j.1365-2966.2005.09451.x)

Kewley, L. J., Dopita, M. A., Sutherland, R. S., Heisler, C. A., & Trevena, J. 2001, ApJ, 556, 121, doi: [10.1086/321545](https://doi.org/10.1086/321545)

Kewley, L. J., Geller, M. J., & Barton, E. J. 2006, AJ, 131, 2004, doi: [10.1086/500295](https://doi.org/10.1086/500295)

Kim, S., Rey, S.-C., Jerjen, H., et al. 2014, ApJS, 215, 22, doi: [10.1088/0067-0049/215/2/22](https://doi.org/10.1088/0067-0049/215/2/22)

Kim, S., Rey, S.-C., Bureau, M., et al. 2016, ApJ, 833, 207, doi: [10.3847/1538-4357/833/2/207](https://doi.org/10.3847/1538-4357/833/2/207)

Kleiner, D., Pimbblet, K. A., Jones, D. H., Koribalski, B. S., & Serra, P. 2017, MNRAS, 466, 4692, doi: [10.1093/mnras/stw3328](https://doi.org/10.1093/mnras/stw3328)

Komatsu, E., Smith, K. M., Dunkley, J., et al. 2011, ApJS, 192, 18, doi: [10.1088/0067-0049/192/2/18](https://doi.org/10.1088/0067-0049/192/2/18)

Kraljic, K., Arnouts, S., Pichon, C., et al. 2018, MNRAS, 474, 547, doi: [10.1093/mnras/stx2638](https://doi.org/10.1093/mnras/stx2638)

Kuutma, T., Tamm, A., & Tempel, E. 2017, A&A, 600, L6, doi: [10.1051/0004-6361/201730526](https://doi.org/10.1051/0004-6361/201730526)

Larson, R. B., Tinsley, B. M., & Caldwell, C. N. 1980, ApJ, 237, 692, doi: [10.1086/157917](https://doi.org/10.1086/157917)

Luber, N., van Gorkom, J. H., Hess, K. M., et al. 2019, AJ, 157, 254, doi: [10.3847/1538-3881/ab1b6e](https://doi.org/10.3847/1538-3881/ab1b6e)

Mahajan, S. 2013, MNRAS, 431, L117, doi: [10.1093/mnrasl/slt021](https://doi.org/10.1093/mnrasl/slt021)

Mahajan, S., Singh, A., & Shobhana, D. 2018, MNRAS, 478, 4336, doi: [10.1093/mnras/sty1370](https://doi.org/10.1093/mnras/sty1370)

Malavasi, N., Arnouts, S., Vibert, D., et al. 2017, MNRAS, 465, 3817, doi: [10.1093/mnras/stw2864](https://doi.org/10.1093/mnras/stw2864)

Martínez, H. J., Muriel, H., & Coenda, V. 2016, MNRAS, 455, 127, doi: [10.1093/mnras/stv2295](https://doi.org/10.1093/mnras/stv2295)

Martizzi, D., Vogelsberger, M., Artale, M. C., et al. 2019, MNRAS, 486, 3766, doi: [10.1093/mnras/stz1106](https://doi.org/10.1093/mnras/stz1106)

Mei, S., Blakeslee, J. P., Côté, P., et al. 2007, ApJ, 655, 144, doi: [10.1086/509598](https://doi.org/10.1086/509598)

Mihos, J. C., & Hernquist, L. 1994, ApJL, 431, L9, doi: [10.1086/187460](https://doi.org/10.1086/187460)

—. 1996, ApJ, 464, 641, doi: [10.1086/177353](https://doi.org/10.1086/177353)

Parekh, V., Durret, F., Padmanabh, P., & Pandge, M. B. 2017, MNRAS, 470, 3742, doi: [10.1093/mnras/stx1457](https://doi.org/10.1093/mnras/stx1457)

Peng, Y.-j., Lilly, S. J., Kovač, K., et al. 2010, ApJ, 721, 193, doi: [10.1088/0004-637X/721/1/193](https://doi.org/10.1088/0004-637X/721/1/193)

Popping, A., Davé, R., Braun, R., & Oppenheimer, B. D. 2009, A&A, 504, 15, doi: [10.1051/0004-6361/200911811](https://doi.org/10.1051/0004-6361/200911811)

Praton, E. A., & Schneider, S. E. 1994, ApJ, 422, 46, doi: [10.1086/173702](https://doi.org/10.1086/173702)

Robotham, A. S. G., Liske, J., Driver, S. P., et al. 2013, MNRAS, 431, 167, doi: [10.1093/mnras/stt156](https://doi.org/10.1093/mnras/stt156)

Sancisi, R., Fraternali, F., Oosterloo, T., & van der Hulst, T. 2008, A&A Rv, 15, 189, doi: [10.1007/s00159-008-0010-0](https://doi.org/10.1007/s00159-008-0010-0)

Sarron, F., Adamo, C., Durret, F., & Laigle, C. 2019, A&A, 632, A49, doi: [10.1051/0004-6361/201935394](https://doi.org/10.1051/0004-6361/201935394)

Springel, V., White, S. D. M., Jenkins, A., et al. 2005, Nature, 435, 629, doi: [10.1038/nature03597](https://doi.org/10.1038/nature03597)

Tanimura, H., Hinshaw, G., McCarthy, I. G., et al. 2019, MNRAS, 483, 223, doi: [10.1093/mnras/sty3118](https://doi.org/10.1093/mnras/sty3118)

Tonnesen, S., Bryan, G. L., & van Gorkom, J. H. 2007, ApJ, 671, 1434, doi: [10.1086/523034](https://doi.org/10.1086/523034)

Vulcani, B., Poggianti, B. M., Oemler, A., et al. 2013, A&A, 550, A58, doi: [10.1051/0004-6361/201118388](https://doi.org/10.1051/0004-6361/201118388)

Wetzel, A. R., Tinker, J. L., & Conroy, C. 2012, MNRAS, 424, 232, doi: [10.1111/j.1365-2966.2012.21188.x](https://doi.org/10.1111/j.1365-2966.2012.21188.x)

Wyder, T. K., Martin, D. C., Schiminovich, D., et al. 2007, ApJS, 173, 293, doi: [10.1086/521402](https://doi.org/10.1086/521402)

Zabludoff, A. I., Zaritsky, D., Lin, H., et al. 1996, ApJ, 466, 104, doi: [10.1086/177495](https://doi.org/10.1086/177495)